



RESEARCH ARTICLE

10.1002/2016WR020024

Validating a universal model of particle transport lengths with laboratory measurements of suspended grain motions

Suleyman Naqshband^{1,2} , Brandon McElroy¹ , and Robert C. Mahon¹ ¹Department of Geology and Geophysics, University of Wyoming, Laramie, Wyoming, USA, ²Hydrology and Quantitative Water Management Group, Wageningen University and Research Centre, Wageningen, Netherlands

Key Points:

- This research presents a universal model for particle transport lengths
- Unique particle motion is recorded for the first time over large distances using a series of eight video cameras
- The presented model can be used to calculate sediment fluxes for a wide range of flow conditions

Supporting Information:

- Supporting Information S1
- Data Set S1
- Data Set S2
- Data Set S3
- Movie S1
- Movie S2

Correspondence to:

S. Naqshband,
SNaqshba@uwyo.edu

Citation:

Naqshband, S., B. McElroy, and R. C. Mahon (2017), Validating a universal model of particle transport lengths with laboratory measurements of suspended grain motions, *Water Resour. Res.*, 53, doi:10.1002/2016WR020024.

Received 27 OCT 2016

Accepted 29 APR 2017

Accepted article online 8 MAY 2017

Abstract The mechanics of sediment transport are of fundamental importance for fluvio-deltaic morphodynamics. The present study focuses on quantifying particle motions and trajectories across a wide range of flow conditions. In particular, a continuous model is presented that predicts particle travel distances for saltation and suspension based on Rouse number and relative grain roughness. By utilizing a series of eight video cameras in a plexiglass flume direct measurements of the distributions of particle travel distances (excursion lengths) were obtained. To this end, experiments were carried out in dark under black lights with fluorescent painted plastic and quartz sand particles. For relatively high Rouse numbers indicating bed load dominant transport regime ($P \geq 2.5$), particle motion is governed by the effect of gravitational forces (settling velocities) and measured excursion lengths closely follow a Gaussian distribution. For $P=2.5$, particle motion is equally subjected to both gravitational and turbulent forces. Consequently, measured excursion lengths exhibit a bimodal distribution with two distinct peaks. As turbulent fluctuations increase and dominate particle motion over gravity ($P < 2.5$), distributions of excursion lengths become unimodal and negative-skewed with mean values deviating from the modes. The predicted trend of linearly increasing excursion lengths with decreasing Rouse numbers is consistent with measured excursion lengths across a wide range of Rouse numbers ($P=1.8-8.9$). Furthermore, measured excursion lengths are observed to fit within the predicted range of excursion lengths with no significant difference between measured excursion lengths of plastic and quartz sand particles.

1. Introduction

Due to the complex interaction of flow and sediment, river beds exhibit wavy and dynamic morphology that is essential for determining hydraulic roughness and water levels. Transport of sediment is classically broken down into two distinct modes: bed material load and wash load. Wash load is transport of fine sediment that does not usually contribute to the morphological development of an alluvial river bed. Bed material load consists of sediment that originates on the bed and moves in regular contact with the bed through bed load trajectories and through flights of suspension (suspended load) [Naqshband *et al.*, 2015].

Bed material load represents an important fraction of the total sediment flux transported in rivers and it determines many morphological aspects in rivers, including bank erosion, bed form growth, and migration, and the rate at which the river incises relief [e.g., *Yalin and Ferreira da Silva*, 2001 and references therein]. Particles in bed load travel either in traction (rolling and sliding when the fluid shear stress just exceeds the threshold of motion) or saltation (ballistic hops that are controlled by grain size, mean shear stress, and bed roughness) with saltation being the dominant mode of bed load transport in natural rivers [Hu and Hui, 1996]. Particle saltation is confined to a layer with a maximum thickness of 10 particle diameter where particle motion is dominated by the effect of gravitational forces resulting into regular particle hops (see Figure 1a) [Van Rijn, 1984]. Particles obtain their momentum from skin friction and flow pressure originating from velocity gradient near-bed. Horizontal distance (hop or saltation lengths λ_b) that saltating particles travel between successive hops is on the order of 10–100 times the average grain diameter [Wiberg and Smith, 1987; Claudin *et al.*, 2011].

Suspended load is the transport of sediment above the bed in intermittent suspension when the value of bed shear stress exceeds fall velocity of grains. Suspended load plays a crucial role in several aspects of morphological changes in rivers, including bed form decay and bed form transition under high flow conditions [Naqshband *et al.*, 2014], promoting the occurrence of patterns such as bars, antidunes, and meanders with

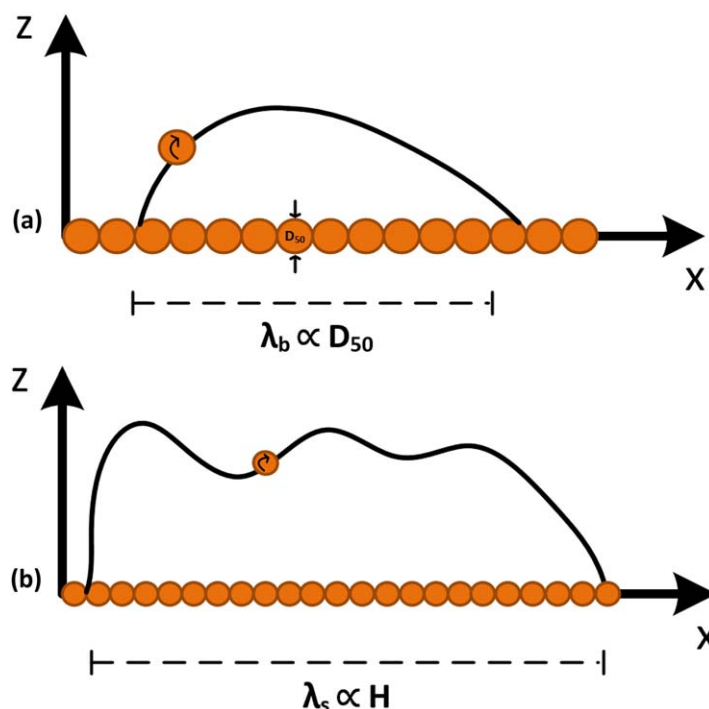


Figure 1. (a) Definition sketch of saltating bed load particle with λ_b saltation or hop length that scales with mean grain diameter D_{50} and (b) suspended load particle motion with λ_s particle excursion length that scales with mean water depth H , adopted from Naqshband and McElroy [2016].

large wavelengths [Claudin *et al.*, 2011], advancing low angle dunes [Hendershot *et al.*, 2016] and low angle delta foresets [e.g., Jopling, 1963]. While saltating bed load particles show—to a great extent—regular hops strictly due to the effect of gravity forces (Figure 1a), suspended load particle motion is substantially more irregular due to random succession of upward impulses imparted by interactions of grains with turbulent eddies (Figure 1b) [Baginold, 1973]. Horizontal distances that suspended particles travel between successive flights (start to stop)—hereafter referred to as the excursion lengths λ_s —scales with water depth and is typically several meters in flumes and potentially up to tens of kilometers in natural rivers [Claudin *et al.*, 2011]. In the present study, excursion length is defined as streamwise distance between the point where particles are released into the flow and the point where particles hit the flume bed for the first time.

Sediment transport has been addressed in various scales over the last century. The classical, reach-scale approach is to predict average sediment discharge as a function of flow strength (e.g. bed shear stress). Empirical relations between sediment discharge and flow strength are derived by means of regression from data acquired in flume experiments [e.g., Meyer-Peter and Muller, 1948; Engelund and Hansen, 1967; Fernandez-Luque and van Beek, 1976]. Although this approach has been shown to correctly describe sediment discharge for steady, uniform, or gently varying flows [e.g., Julien, 1994; Ancey *et al.*, 2008], due to simplifications of physical mechanisms governing particle motion, it fails to provide accurate predictions for conditions that depart from steady uniform flow, such as flows over arbitrarily sloping beds [e.g., Seminara *et al.*, 2002]. Sediment discharge measured in natural streams are generally found to be more than an order of magnitude lower compared to the empirical flume-based transport equations [Wilcock, 2001; Bathurst, 2007; Hergault *et al.*, 2010].

In order to better understand the complex processes of sediment transport and to provide accurate predictions under various flow and bed conditions, many researchers have considered sediment transport not as a flux of continuous phase that has resulted in the traditional flume-based sediment transport equations but as the superimposition of the motion of individual grains. Accordingly, numerous experimental and numerical studies over the past decades have aimed to describe sediment transport at grain scale and in particular to quantify grain trajectory and motion by investigating different physical processes such as collision-rebound of grains with the bed [Schmeeckle *et al.*, 2001], hydrodynamic lift forces and turbulence effects on grains [Bridge and Bennett, 1992; Niño *et al.*, 1994], grain lift-off and impact angle at the bed and rotation (Magnus force) [White and Schultz, 1977; Niño and Garcia, 1998; Lee and Hsu, 1996; Mazumder *et al.*, 2008].

An overwhelming majority of these studies have addressed bed load mechanics under relatively low flow conditions focusing on grain saltation characteristics. By applying photographic techniques in flumes and by developing both deterministic and probabilistic models, quantitative information is provided on the

exact shape of saltation trajectories including distribution of particle velocities, accelerations, hop, or saltation lengths and travel times. *Francis* [1973] was the first to study single particle motion over fixed bed by recording images of saltating particles at a rate of 40 fps followed by *Abbott and Francis* [1977], *Drake et al.* [1988], *Niño et al.* [1994], *Lee and Hsu* [1994], and later *Niño and Garcia* [1998] who applied a high-speed video system recording images at a rate of 250 fps which enabled them to expose particle resting time between successive saltations, particle reentrainment into saltation and particle rotation and associated transverse motion of the particles during successive hops. More recently, *Lajeunesse et al.* [2010] and *Bhattacharyya et al.* [2013] investigated trajectories of saltating particles and measured particle velocity as well as surface density of moving particles where the later also varied bed roughness by gluing different grain sizes on the fixed bed. In addition to fixed bed investigations, particle saltation has been studied over mobile beds [*Fernandez-Luque and van Beek*, 1976; *Van Rijn*, 1984; *Niño and Garcia*, 1994] resulting in numerous empirical as well as parameterized models describing particle saltation characteristics (saltation height, length, velocity, and acceleration) as a function of flow and sediment conditions. For a detailed overview of these models, see *Naqshband and McElroy* [2016].

In addition to experimental investigations, several (detailed) numerical models were developed that focused on accurate description of the shape of a single saltation trajectory through accounting for the impact of one or more individual processes such as: collision-rebound between particles [*Schmeeckle et al.*, 2001; *Lee et al.*, 2002; *Bialik*, 2011], particle collision-rebound with the channel bottom [*Sekine and Kikkawa*, 1992; *Niño and Garcia*, 1994], three-dimensional nature of the particles' motion [*Lee et al.*, 2006; *Bialik et al.*, 2012], hydrodynamic lift force acting on the particles [*Lee and Hsu*, 1996; *Zou et al.*, 2007; *Lukerchenko et al.*, 2008], and drifting force due to turbulent diffusion [*Rowiński*, 1995]. For additional details on these models, see the recent review work of *Bialik* [2015] on Lagrangian models of saltating sediment transport.

More recently, probabilistic approaches to bed load transport have received growing attention from the scientific community [e.g., *Ancey*, 2010; *Furbish et al.*, 2012a, 2012c, 2016; *Heyman et al.*, 2014; *Fathel et al.*, 2015]. Particle motions and positions are treated as stochastic quantities by assuming probability density functions for the instantaneous velocities and accelerations of particles, and their hop lengths and associated travel times (measured start-to-stop). The result is a flux form of the Master equation (a general expression of conservation) where volumetric flux consists of an advective part (similar to the classical description of average flux calculated as the product of mean velocity and concentration) and a diffusive part associated with variations in particle positions and motions [e.g., *Furbish et al.*, 2012a]. The diffusive part of the flux vanishes for steady, uniform flows (planar bed) but might have a dominant contribution to the total flux in the case of unsteady morphodynamics such as bars and bed forms [*Jermolmack and Mohrig*, 2005; *Furbish et al.*, 2012a]. A significant challenge in this probabilistic approach of sediment transport is to predict or assume an appropriate form of the probability density functions for the quantities describing particle motion, and most importantly the distribution of particle hop lengths. Typically the forms of these distributions are estimated from experimental measurements through high-speed imaging and particle tracking [e.g., *Lajeunesse et al.*, 2010; *Roseberry et al.*, 2012; *Heyman*, 2014; *Fathel et al.*, 2015]. However, due to limited availability of experimental data and conditions, descriptions of distributions of particle travel lengths for a wide range of flow conditions are yet forthcoming [*Furbish et al.*, 2016].

As discussed above, sediment transport studies at grain scale have been limited to relatively low flow conditions investigating bed load mechanics (saltation characteristics) while characteristics of suspended grain motion—primarily due to the large distances that suspended particles travel once they are picked up from the bed—have not yet been directly quantified. Although several researchers have attempted to derive equations for average or characteristic excursion length of suspended sediment particles as a function of flow strength and sediment characteristics (see section 2.1), none of these relationships could be compared with direct measurements of particle excursion lengths. Consequently, empirical relationships between excursion lengths and flow conditions remain largely unexplored limiting the application of particle motion equations to bed load dominant cases under low flow conditions.

Within this context, the aim of this paper is to present a continuous, validated model that predicts the distribution of particle saltation and excursion lengths as a function of flow strength and sediment characteristics for both bed load and suspended load dominant transport conditions. Our approach involves modeling

particle saltation and excursion lengths in a single framework using identical parameters for flow strength and sediment characteristics. Furthermore, utilizing a series of eight synchronized video cameras viewing into a plexiglass flume over a streamwise distance of 1.60 m, novel measurements of particle motions and trajectories were obtained across a wide range of flow conditions resulting in direct measurements of the distribution of particle excursion lengths. To this end, experiments were carried out in dark under black lights with fluorescent painted plastic and sand particles.

The paper is organized as follows. Section 2 presents the continuous, theoretical-empirical model for the distribution of particle saltation and excursion lengths. This includes derivation of an excursion length model from traditional advection-settling model that predicts the characteristic suspended particle advection length-scale. A saltation model is derived by applying a polynomial fit to existing saltation data from literature using the identical parameter framework that is used to describe particle suspension excursion lengths. Section 3 outlines the experimental work including setup of the cameras and measuring procedure. Data analysis and processing is concisely discussed followed by experimental conditions. The measured distributions of particle excursion length are presented in section 4 and subsequently compared with the derived excursion length model across flow conditions. Implications and possible future applications of this study are discussed in section 5.

2. A Continuous Model for Particle Saltation and Excursion Lengths

2.1. Excursion Length Model

Because measuring suspended particle travel lengths (excursion lengths) for individual particles directly has not yet been accomplished, many studies have derived a characteristic particle excursion length-scale by considering differential equations that relate mass conservation to vertical entrainment and settling rates of particles [Einstein, 1950; Parker, 1978; Paola and Voller, 2005; Lamb et al., 2010; Claudin et al., 2011]. By assuming net-zero entrainment deposition rate from the bed and that settling rates do not change, an advection-saturation length-scale of suspended particle l_a (m) is derived from the entrainment-deposition based Exner equation (equation (1)) where ε is porosity of the bed, η (m) denotes the bed elevation, t (s) is time, w_s (m s^{-1}) is the particle settling velocity, E is a dimensionless entrainment parameter, and c_b denotes the near-bed sediment concentration.

$$(1-\varepsilon)\frac{\partial\eta}{\partial t} = -w_s(E-c_b) \quad (1)$$

The volume rate of entrainment of bed particles into suspension is w_sE and w_sc_b represents the volume rate of deposition of suspended load onto the bed. Under equilibrium conditions, the dimensionless entrainment parameter equals the near-bed sediment concentration. Applying the definitions $r_0 = c_b/c$ (ratio between near-bed sediment concentration and depth-averaged sediment concentration) and $q_s = qc$ (sediment discharge q_s equals the product of flow discharge q and depth-averaged sediment concentration) results in equation (2).

$$(1-\varepsilon)\frac{\partial\eta}{\partial t} = -\frac{w_sr_0}{q}(q_{se}-q_s) \quad (2)$$

$$(1-\varepsilon)\frac{\partial\eta}{\partial t} = \frac{q_s-q_{se}}{l_a}$$

The parameter $r_0 \geq 1$ describes the vertical sediment stratification which may have a relatively constant value between 1.5 and 2 across a wide range of stress conditions [Parker et al., 1987]. Under high flow conditions where density stratification significantly affects total suspended load and size distribution, r_0 might be much larger than 2 [Wright and Parker, 2004]. The advection-saturation length-scale $l_a = q/r_0w_s$ (m) represents the length over which the suspended sediment transport relaxes toward its saturation or equilibrium value q_{se} . This and similar suspended sediment length-scales are shown to be important in the context of geomorphology; bed form stability [Mohrig and Smith, 1996; Davy and Lague, 2009], turbidity currents [Dade and Huppert, 1994; Straub and Mohrig, 2008; Lamb et al., 2010], and aeolian sediment transport [Claudin et al., 2011; Andreotti et al., 2010].

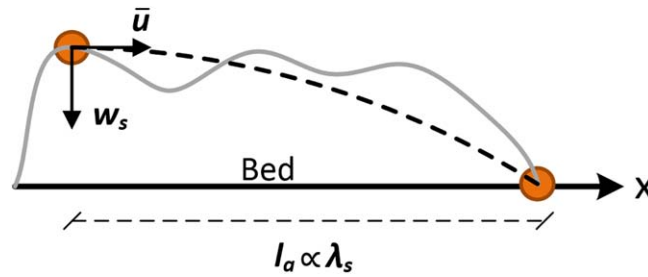


Figure 2. Definition sketch of suspended particle advection length-scale l_a (dotted black) and suspended particle excursion length (solid gray).

water depth H . Recognizing that $q = \bar{u}H$ where \bar{u} is depth-averaged flow velocity, the dimensionless excursion length is given by

$$l^* = \frac{\lambda_s}{H} = \frac{\bar{u}}{r_0 w_s} \quad (3)$$

The next step is to introduce an expression for depth-averaged flow velocity (equation (4)) derived from the law-of-the-wall velocity profile where u_* (m s^{-1}) is bed shear velocity, $\kappa = 0.4$ is von Karman's constant, D_{50} (m) is median grain size and A_s describes bed roughness as a function of shear Reynolds number.

$$\bar{u} = \frac{u_*}{\kappa} \left[\ln \left(A_s \frac{H}{D_{50}} \right) - 1 \right] \quad (4)$$

Combining (3) and (4) results in the following equation for dimensionless excursion length

$$l^* = \frac{u_*}{r_0 w_s \kappa} \left[\ln \left(A_s \frac{H}{D_{50}} \right) - 1 \right] \quad (5)$$

Recognizing Rouse number as the ratio of particle settling velocity and bed shear velocity, $P = w_s / \kappa u_*$, and recognizing relative grain roughness as the ratio of mean grain diameter and water depth $D^* = D_{50} / H$, dimensionless excursion length in (5) can be written as follows:

$$l^*(P, D^*) = \frac{1}{r_0 \kappa^2 P} \left[\ln \left(\frac{A_s}{D^*} \right) - 1 \right] \quad (6)$$

The end result in equation (6) is an expression for dimensionless excursion length l^* as a function of water depth, shear velocity, grain size, and grain settling velocity through Rouse number P and relative grain roughness D^* .

As expected from inspection of equation (6) with $r_0 = 2.0$ [Parker et al., 1987; Garcia, 1994; Lamb et al., 2010], excursion lengths increase linearly with decreasing Rouse numbers indicating greater flow strength and/or smaller settling velocities (Figure 3). Excursion lengths also increase for decreasing relative grain roughness indicating smaller particle diameter and/or greater flow depth, but the relative increase is much smaller. This suggests that average distance travelled by suspended particles is prominently governed by flow strength and sediment fall velocities [e.g., Bagnold, 1973].

For typical sandy rivers with Rouse numbers that vary between 0.5 and 5 and relative grain roughness in the order of 10^{-4} [Naqshband et al., 2014], equation (6) predicts average suspended particle travel lengths of 5 up to 100 times the average water depth. Whereas for typical flume conditions with similar Rouse numbers and sediment sizes, mean particle excursion lengths predicted from equation (6) are in the range of 2–40 times the average water depth. The reason for this is an order of magnitude larger value of relative grain roughness due to limited flow depths in flumes (10^{-3}).

2.2. Saltation Length Model

In order to obtain a continuous model across a wide range of flow and sediment conditions for both bed load saltation and suspended load excursion lengths, the parameter framework $l^*(P, D^*)$ used in section 2.1 to describe excursion lengths is applied to saltation length data from literature. Table 1 shows an overview

Furthermore, particle advection-saturation length-scale is found to be proportional to particle excursion length λ_s (see Figure 2) [e.g., Abbott and Francis, 1977; Wiberg and Smith, 1987]. In the present study, we use this as a starting point for our excursion length model.

In order to make predictions of excursion lengths across different scales, a dimensionless excursion length l^* is defined by normalizing $l_a \approx \lambda_s$ with

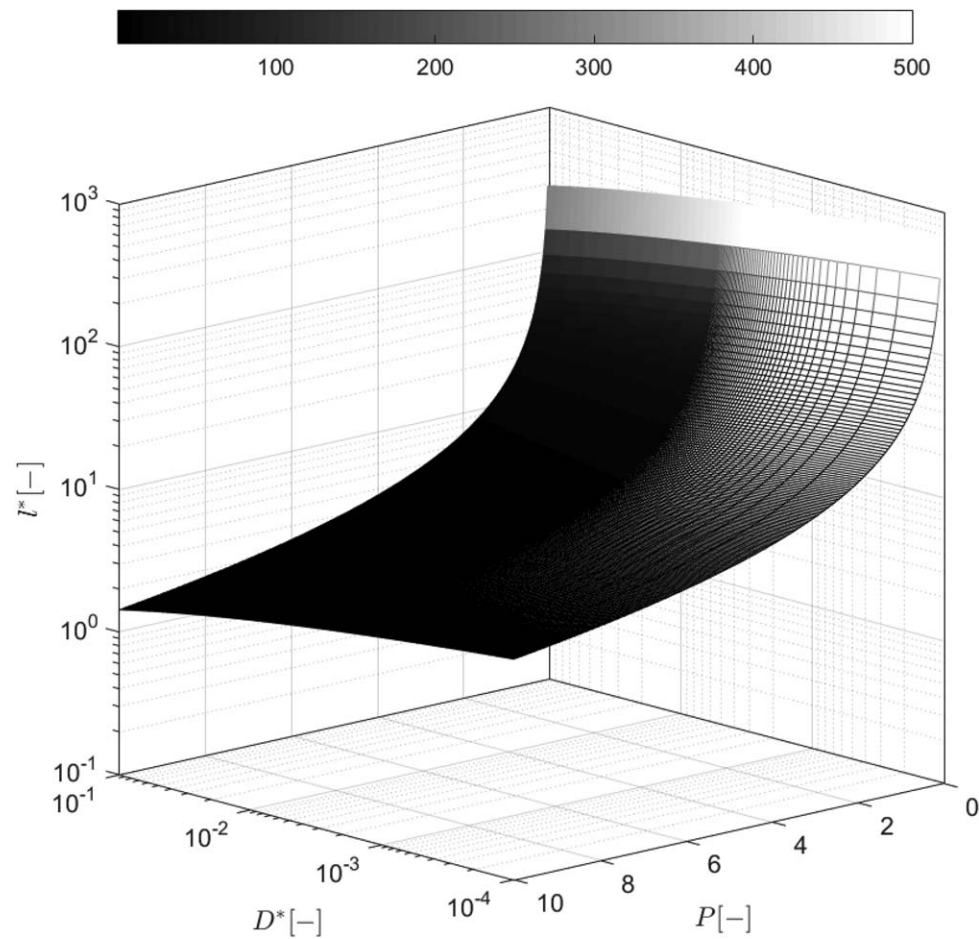


Figure 3. Dimensionless excursion length l^* as a function Rouse number P and relative grain roughness D^* based on derived model in equation (6).

of six saltation length data sets that are selected from literature such that a wide range of flow and sediment conditions are represented including a total of 54 individual experiments. First, bed load saltation length is normalized with water depth $l^* = \lambda_b/H$. Subsequently, dimensionless saltation lengths l^* for all data sets are plotted as a function of Rouse number P and relative grain roughness D^* (see Figure 4, red dots). Next, a polynomial surface fit is applied to all data points ($R^2=0.88$) resulting in the following equation for dimensionless saltation lengths with $\alpha=-0.24$, $\beta=6.73$, and $\gamma=5.86$.

$$l^*(P, D^*) = \alpha P + \beta D^* + \gamma \tag{7}$$

Similar to dimensionless excursion lengths (Figure 3), dimensionless saltation lengths (Figure 4) also increase both with decreasing Rouse numbers and decreasing relative grain roughness. However, the relative increase in dimensionless saltation lengths is much larger with decreasing relative grain roughness as

Table 1. Summary of Selected Saltation Data Sets With Range of Parameter's

Data Source	Bed Type	τ_c^* (Pa)	τ^* (Pa)	λ_b/D_{50}	P	D^*	l^*
Abbott and Francis [1977]	Plane bed	0.050	1.04–2.52	10.1–24.2	3.6–9.7	0.17	0.57–4.18
Sekine and Kikkawa [1992]	Mobile alluvial	0.030	0.05–0.55	49.4–294.4	8.7–15.2	0.003–0.013	0.13–1.92
Lee and Hsu [1994]	Fixed alluvial	0.031	1.29–11.0	32.4–105.0	6.0–17.6	0.01–0.04	0.16–2.25
Hu and Hui [1996]	Smooth plane bed	0.030	0.68–3.55	30.0–90.7	1.8–14.2	0.02–0.04	0.49–2.63
Lee et al. [2000]	Fixed alluvial	0.037	1.49–3.97	11.3–37.6	3.1–9.2	0.12	1.36–4.51
Chatanantavet et al. [2013]	Smooth plexiglas	0.007	1.21–4.21	6.6–26.8	2.0–12.6	0.11–0.98	2.00–9.08

For additional details reference is made to Chatanantavet et al. [2013].

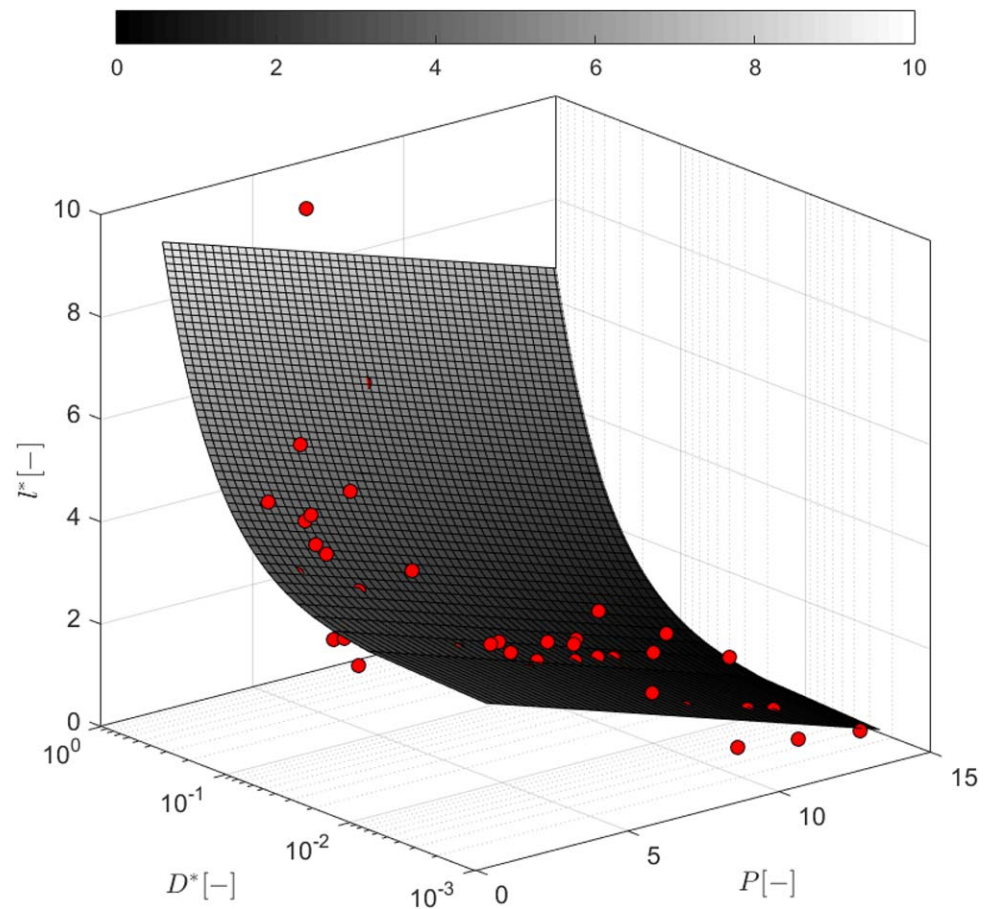


Figure 4. Polynomial surface fit through particle saltation data from literature (red dots, Table 1) in Rouse number P and relative grain roughness D^* parameter framework (see equation (7)).

expected from equation (7). This means that averaged distance travelled by saltating particles is mainly controlled by particle size that gives rise to drag and lift forces rather than particle fall velocities or flow strength as saltating particles remain very close to the bed in the viscous boundary layer [e.g., Wiberg and Smith, 1987].

2.3. Combining Saltation and Excursion Length Models Into One Continuous Model

Figure 5 shows both saltation length (black surface) and excursion length (red surface) models in the l^* (P, D^*) parameter framework. The models intersect for Rouse numbers P varying between 0.5 and 6.5. For high values of P reflecting low to moderate flows, saltation is the dominant mode of transport (black surface) whereas for low values of P grains moving in suspension becomes dominant (red surface). Although many studies have argued that saltation is the dominant mode of transport for p values exceeding 2.5, and that transport of particles in suspension becomes dominant for $P < 2.5$ [e.g., Van Rijn, 1993], Figure 5 indicates that this transition depends on relative grain roughness D^* . The transition between transport modes is expected to occur at higher Rouse numbers with decreasing D^* . This means that for large values of D^* (relative large particle size to flow depth ratio), grains remain in saltation for much higher flow strengths than is the case for smaller particle size to flow depth ratios (small D^*). Figure 5 further illustrates possible coexistence of both saltation and suspension modes for widely distributed sediment mixtures; depending on D^* , both transport modes are present for p values between 0.5 and 6.5.

Figure 6 shows two continuous profiles of l^* as a function of Rouse number corresponding to two different values of D^* . The D^* values represent the range of experimental conditions designed to test the derived excursion length model (see Table 1). For $D^* = 2.90e^{-3}$, the mode transition occurs at $P = 5.25$ whereas for

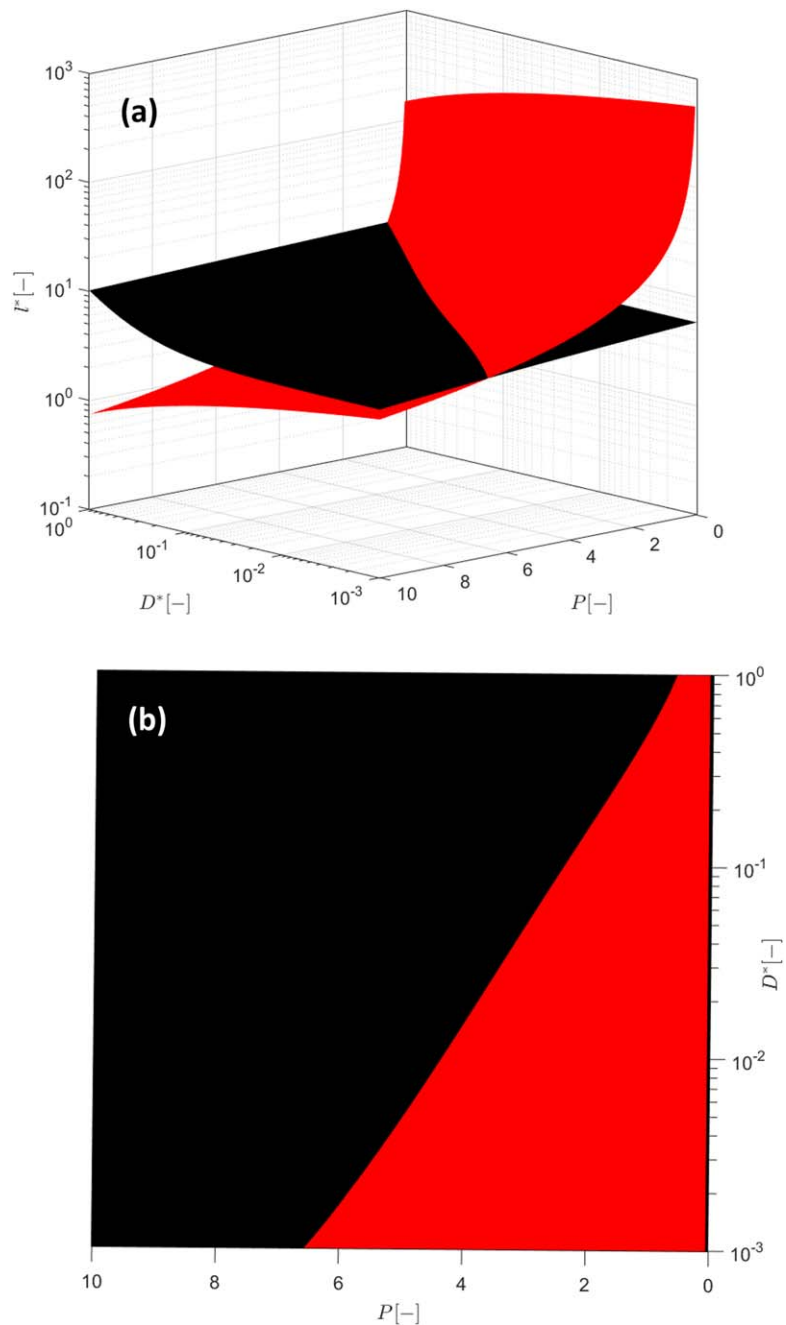


Figure 5. Intersection of excursion (red surface, equation (6)) and saltation (black surface, equation (7)) length models as a function of Rouse number P and relative grain roughness D^* (a) side view and (b) helicopter view. This represents the complete model for sediment transport across a wide range of conditions using a single parameter framework.

$D^* = 1.55e^{-2}$ the transition occurs at $P=4.90$. The dotted lines in Figure 6 illustrate the behavior of excursion length model for high Rouse numbers if the saltation length model is not considered.

3. Experimental Techniques and Methodology

3.1. Setup and Instrumentation

Particle motions and travel lengths were measured for a wide range of flow conditions using a recirculating plexiglass flume at the University of Wyoming (Figure 7a). The flume was 3.25 m \times 0.1 m with an effective measuring section of 2.45 m. A series of eight video cameras (eight channel Full HD-CVI 1080P 2.4MP

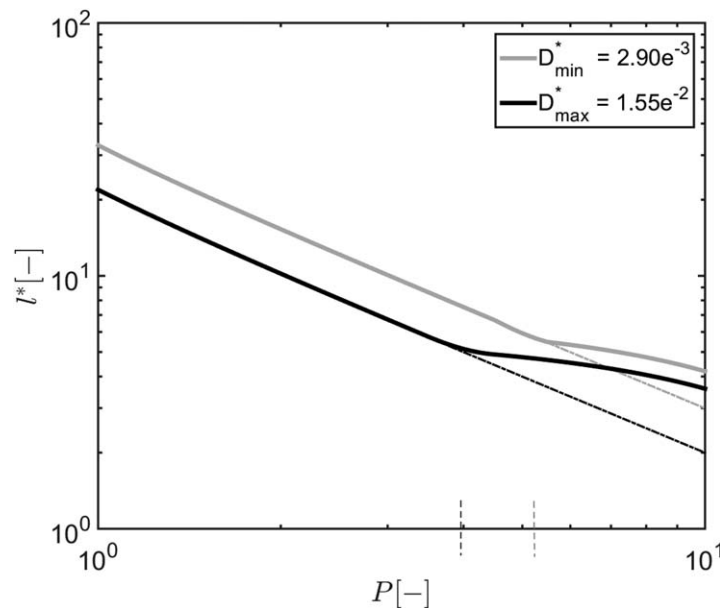


Figure 6. Selected profiles from the continuous particle travel length model for experimentally tested range of relative grain roughness D^* values (see Table 2). The dotted lines show the behavior of excursion length model for the selected D^* values (equation (6)).

sampling rate of 50 Hz over a time period of 100 s. Figure 8a shows logarithmic profiles of mean flow velocities for the measured flow conditions with a constant water depth $h=0.1$ m. Profiles of turbulent Reynolds shear stresses are shown in Figure 8b. Bed shear stress for each flow condition was derived from the maximum value of Reynolds shear stresses at approximately 8 mm from the bed ($z/h=0.08$).

In order to measure particle motion and travel lengths across a wide range of flow and sediment conditions, both sand ($SG = 2.65$) and plastic ($SG = 1.2$) particles were used (Figure 9a). Sand particle diameter range was 0.28–0.50 mm and plastic particle diameter range was 0.42–1.70 mm. Both sand and plastic particles were first painted with fluorescent paint and then sieved into three and seven narrow particle size classes, respectively. The exact particle-size distributions for each class were measured with a Microtrac Dry Image Analyzer. The results for both sand and plastic particles are shown in Figure 9b together with median particle sizes D_{50} . In addition, settling velocities were measured for all 10 sand and plastic particle size classes. For each class, at least 100 particles were inserted in still water and settling velocity distributions were determined over a distance of 0.15 m by tracking individual particles as shown in Figure 9c (see section 3.2 for more details on particle tracking). The distribution of settling velocities for each particle size class is shown in Figure 9d together with mean values and standard deviations.

3.2. Experimental Procedure

Each experiment started with ensuring fully developed equilibrium flow by adjusting flume slope while keeping water depth and pump rate constant. After obtaining equilibrium flow, respective size classes of

camera system) was installed each covering 20.0 cm stream-wise distance of the effective measuring length and 15.0 cm in the vertical by placing a grid in the centerline of the flume where the cameras were focused. Each camera imaged at 25 frames per second with 1080×1920 pixel resolution covering a total length of 1.60 m that provided the basis for tracking particle motions over relatively large distances (Figure 7b). The test section of 1.60 m was located 0.80 m downstream from the flow entrance to optimize for fully developed turbulence.

For 3 flow conditions (U1, U2, and U3), profiles of mean stream-wise flow velocities and turbulent shear stresses were measured with an Acoustic Doppler Velocimeter (ADV Vectrino II) at sam-

Table 2. Flow and Sediment Conditions for Plastic and Sand Grain Experiments

Parameter	Experiments With Plastic Grains									Experiments With Quartz Grains				
	EXP1	EXP2	EXP3	EXP4	EXP5	EXP6	EXP7	EXP8	EXP9	EXP10	EXP11	EXP12	EXP13	EXP14
Water depth h (m)	0.10	0.10	0.10	0.10	0.10	0.10	0.10	0.10	0.10	0.10	0.10	0.10	0.10	0.10
Flume slope $S \times 10^{-3}$	0.5	0.5	1.0	1.2	1.2	1.2	1.2	1.2	1.2	1.0	1.2	1.0	1.2	1.2
Bed shear stress $\tau_b \times 10^{-1}$ (Pa)	1.7	1.7	4.2	5.6	5.6	5.6	5.6	5.6	5.6	4.2	5.6	4.2	5.6	5.6
Bed shear velocity $u^* \times 10^{-2}$ ($m s^{-1}$)	1.3	1.3	2.0	2.4	2.4	2.4	2.4	2.4	2.4	2.0	2.4	2.0	2.4	2.4
Median grain diameter $D_{50} \times 10^{-3}$ (m)	1.55	1.23	1.55	1.55	1.24	1.13	0.79	0.67	0.47	0.45	0.45	0.33	0.33	0.29
Mean settling velocity $w_s \times 10^{-3}$ ($m s^{-1}$)	46.9	38.0	46.9	46.9	38.0	26.1	23.9	21.6	17.3	56.0	56.0	37.0	37.0	30.3
Relative grain roughness $D^* \times 10^{-2}$	1.55	1.24	1.55	1.55	1.24	1.13	0.79	0.67	0.47	0.45	0.45	0.33	0.33	0.29
Rouse number P	8.9	7.2	5.7	5.0	4.0	2.8	2.5	2.3	1.8	6.9	5.9	4.5	3.9	3.2

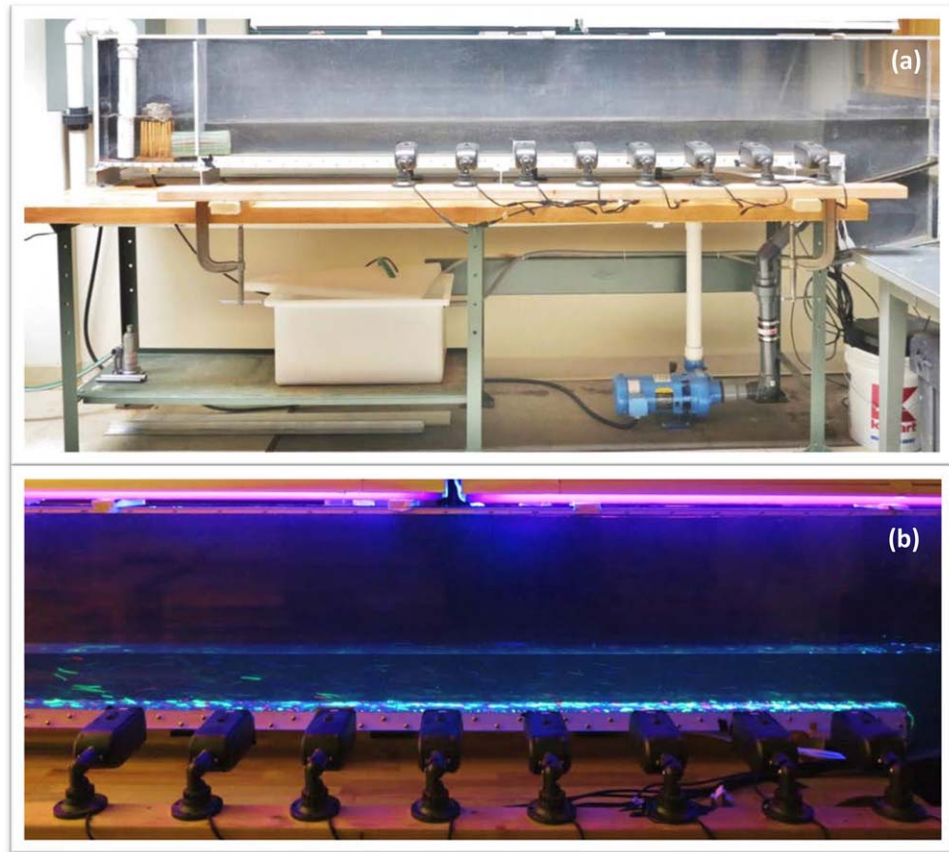


Figure 7. (a) Experimental setup with side view of the Plexiglas flume and (b) installed series of eight synchronized video cameras recording travel paths of fluorescent painted particles under black light. A dynamic video can be accessed in the auxiliary material associated with this figure.

particles were released independently at the centerline of the flume into the view of the most upstream camera. To maintain low particle concentration for particle tracking purposes, a maximum number of 100 particles were released at the same time. Particle motions and trajectories were recorded over a total length

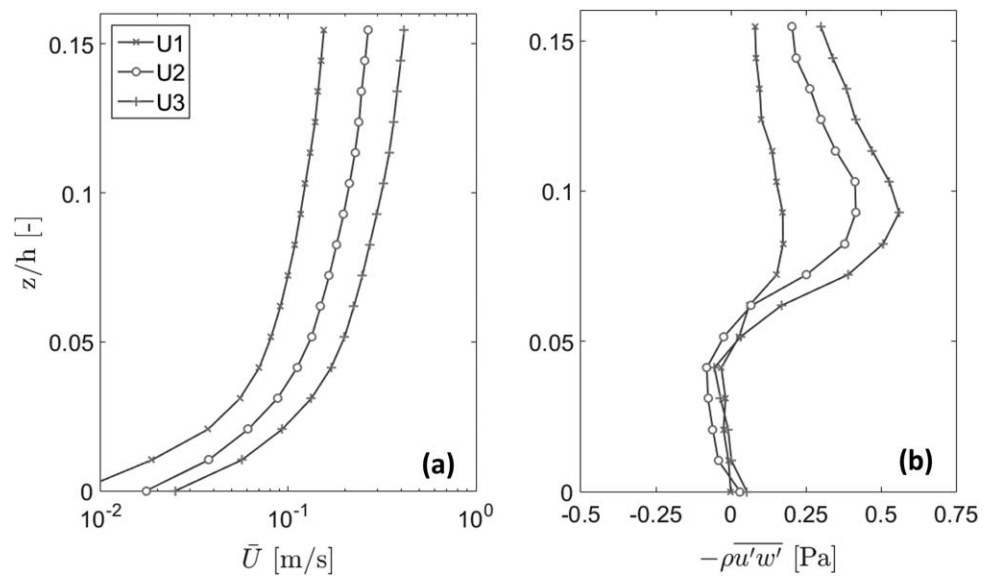


Figure 8. Acoustic Doppler Velocimeter (ADV Vectrino II) measurements showing profiles of (a) mean streamwise flow velocities and (b) Reynolds shear stresses for three different flow conditions.

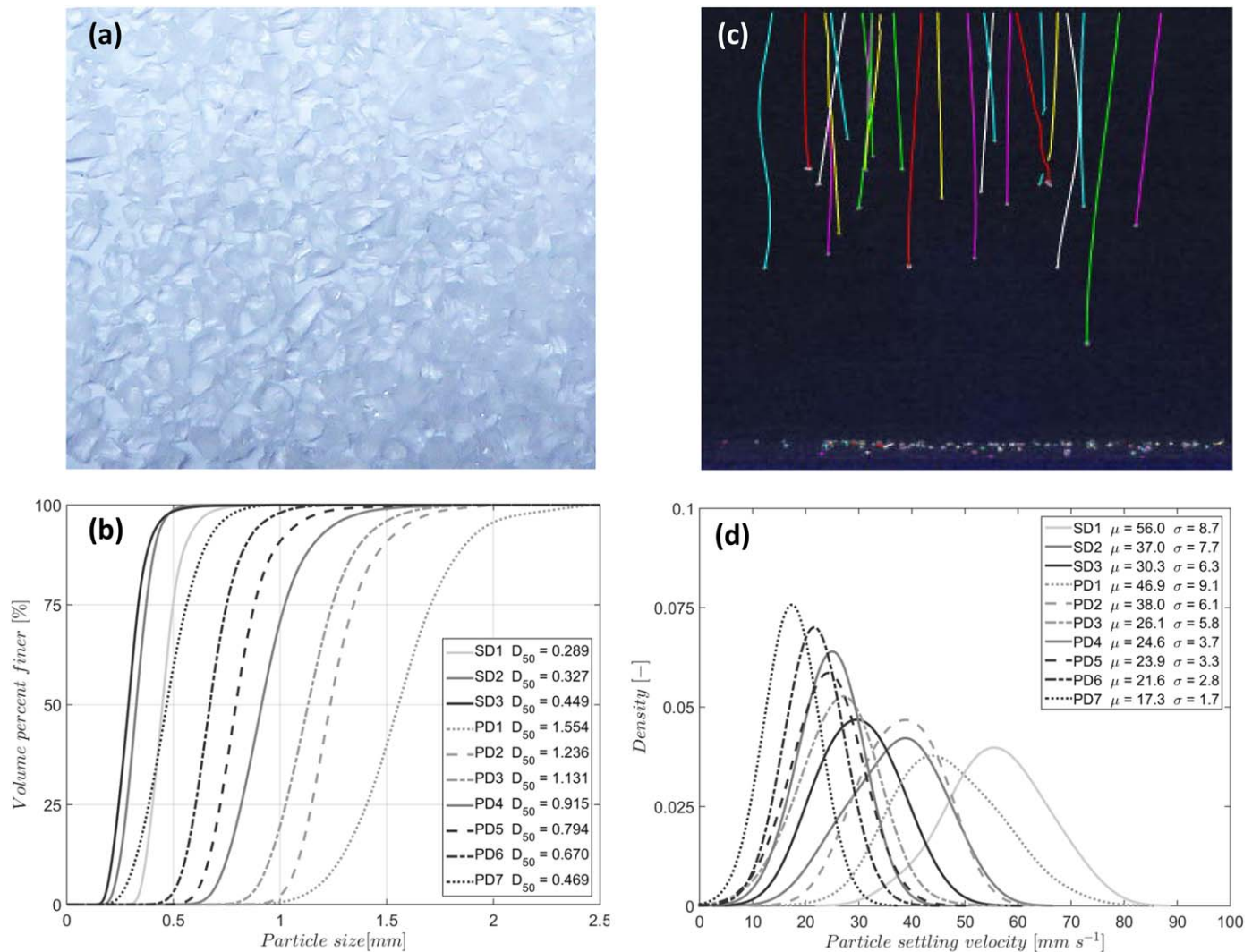


Figure 9. (a) Example of plastic (acrylic) particles used for experimental work, (b) with measured size distributions for plastic (PD) and quartz sand particles shown in. (c) Grain-size distributions of sieved particle classes, and (d) distribution of settling velocities for plastic and sand particles.

of 1.60 m by a series of eight cameras. All experiments were carried out in dark under black lights after both plastic and sand particles were painted with fluorescent spray paint (see Figure 7b). This was done to enhance the contrast of particles so that particles can be easily distinguished and identified from background noise. The plexiglass window at the other side of the flume was covered with a black, thick photographic paper to limit reflection of black lights into the cameras. All eight cameras were synchronized to a subframe resolution by recording a strobe light at the beginning of each experiment. Based on the calculation of grayscale values of recorded images by each camera, the cameras were synchronized with a precision of 1/10 of a frame time. With cameras imaging at 25 frames per second, this means a maximum delay time of 0.004 s between cameras.

Once particle trajectories for each particle size class were recorded and all cameras were synchronized, individual images from each camera were undistorted and stitched together in MATLAB using Image Processing Toolbox. An example of eight stitched images from all cameras is shown in Figure 10a with a resolution of 8640 × 1920 pixels. Next step was to identify each individual particle and track their motions in a sequence of stitched images over the entire length of the effective measuring section. For this purpose, an adapted version of 2-D particle tracking code originally written by Crocker and Grier [1996] was used in MATLAB. The model finds and tracks features based on their characteristics: particle radius, eccentricity, radius of gyration, and intensities. Each feature is uniquely defined and numbered. Next, features are linked into

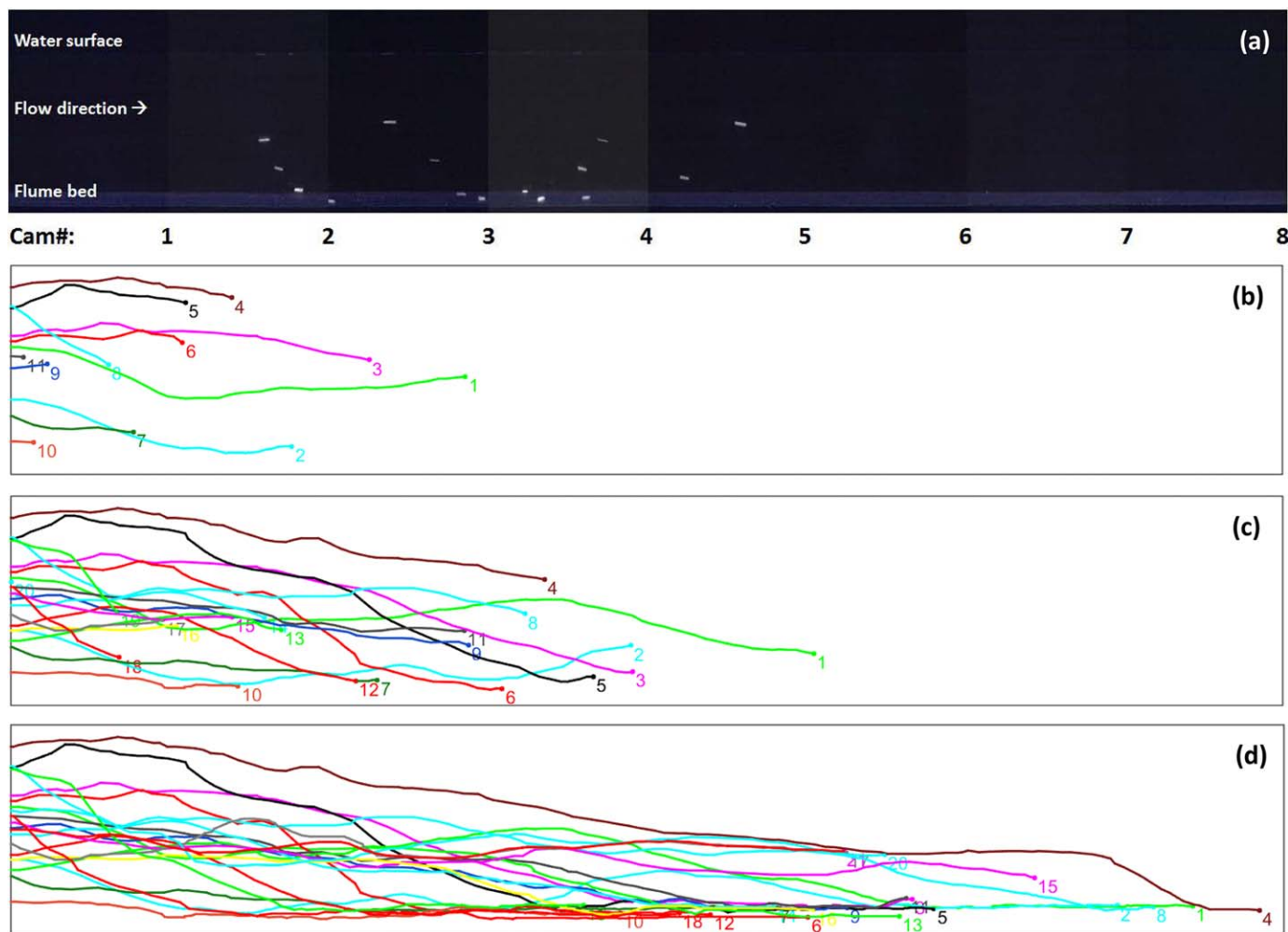


Figure 10. (a) Stacked images of eight video camera’s showing particles as observed under black light and (b–d) individual particle paths identified after particle tracking. A dynamic video can be accessed in the auxiliary material associated with this figure.

trajectories by minimizing the total displacement of individual features between successive frames. The method can be further adapted to allow features skip a certain number of frames and continue linking trajectories when the features reappear. Snapshots of particle trajectories found using particle tracking code are shown in Figure 10. These trajectories are used to extract information about exact particle motions and travel lengths before settling (see section 4). This method is also capable of obtaining information about the distribution of particle velocities, accelerations, and travel times which are not explicitly considered in the present study (see section 5).

3.3. Experimental Conditions

The experimental conditions were designed such that a wide range of Rouse numbers, P , and relative grain roughness, D^* , values were covered. The pixel resolution of the video cameras limited tracking to particles approximately 0.28 mm and larger. In addition, limitations to flow discharge made it impossible to reach Rouse numbers below 3.2 for quartz sand particles (see Table 2). Therefore, plastic particles with a specific gravity of 1.2 kg/m³ were used which allowed us to reach Rouse numbers to 1.8 (see EXP9 in Table 1). Three different flow strengths (Figure 8) were combined with 10 plastic and sand particle size classes to obtain a range of Rouse numbers representing a range of conditions from bed load and suspended load dominant transport modes ($P=1.8–8.9$). For all 14 experiments, water depth was kept constant at 0.1 m and flume slope was adjusted to obtain steady uniform flow over the fixed concrete plane bed. The glass side-walls are estimated to have a Manning’s roughness coefficient of $n=0.010 \text{ s m}^{-1/3}$ [Arcement and Schneider, 1989]. To test our excursion length model derived earlier (see equation (6)), advection-settling lengths of at

least 100 particles were measured for each experimental condition. An overview of flow and sediment conditions for each experiment is shown in Table 2.

4. Results and Discussion

4.1. Distributions of Particle Excursion Lengths

In the bed load dominant transport regime (EXP4, $P=5.0$), particle trajectories are smooth as particle motion is governed by downward settling velocities (Figure 11a). Particles are transported only in saltation as soon as they hit the flume bed (not shown here, see dynamic video in the auxiliary material). In the suspended load dominant regime (EXP8, $P=2.3$), particle trajectories become substantially more irregular as particles are more influenced by random turbulent fluctuations (Figure 11b). Consequently, the spread of distances over which particles hit the flume bed becomes much larger. Particles that contact the bed are subsequently not transported only in saltation but regularly reenter the flow as they are lifted from the bed into suspension (see dynamic video in the auxiliary material: e.g., particle numbers 2, 5, and 11).

Figures 12a and 12b show plots of Kernel density estimations for the distribution of particle excursion lengths measured with plastic (EXP1 through EXP9) and sand (EXP10 through EXP14) particles, respectively. Red dot on each curve indicates mean excursion length for that particular experiment. As expected, mean excursion lengths increase with increasing flow strength (decreasing Rouse numbers, see Table 3). Furthermore, distributions of excursion lengths are observed to become wider with decreasing Rouse numbers for both plastic and sand experiments. This reflects the influence of random turbulent fluctuations on particle motion which is more dominant at relatively low Rouse numbers. For relatively high Rouse numbers indicating bed load dominant transport regime ($P \geq 2.8$) which includes all five experiments with sand particles (EXP10 through EXP14) and first six experiments with plastic particles (EXP1 through EXP6), measured excursion lengths closely follow a Gaussian distribution with distributions being symmetric around their mean values (red dots), and mean values coinciding with the modes. For $P=2.5$ (EXP7), bed load and suspended load transport modes are equally represented and particle motion is governed both by turbulence and gravity (settling velocities). Consequently, measured excursion lengths exhibit a bimodal distribution with two distinct peaks (Figure 12a). As turbulent fluctuations increase and dominate particle motion over gravity ($P < 2.5$), distributions of excursion lengths return to unimodal and are negatively skewed with mean values deviating from the modes (EXP8 and EXP9). For flows fully dominated by turbulent with nearly zero gravitational effects (suspended load dominant transport regime $P < 0.8$), conditions that were not reached in the present study due to instrumental and flume limitations, we hypothesize that excursion lengths will follow a Gaussian distribution similar to distributions under bed load dominated transport regime but possessing a much wider spread.

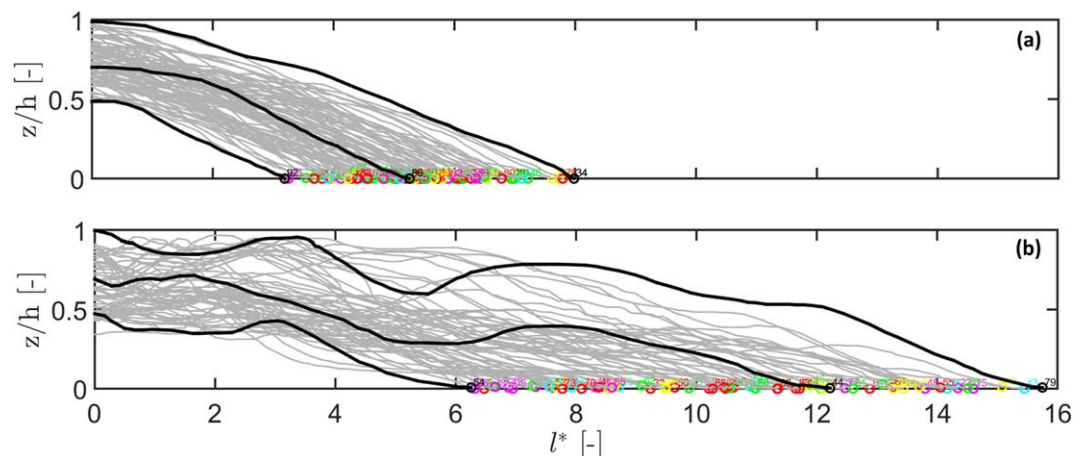


Figure 11. Examples of particle paths measured for (a) EXP4 and (b) EXP8 (b), solid black lines indicate characteristic particle paths for both conditions.

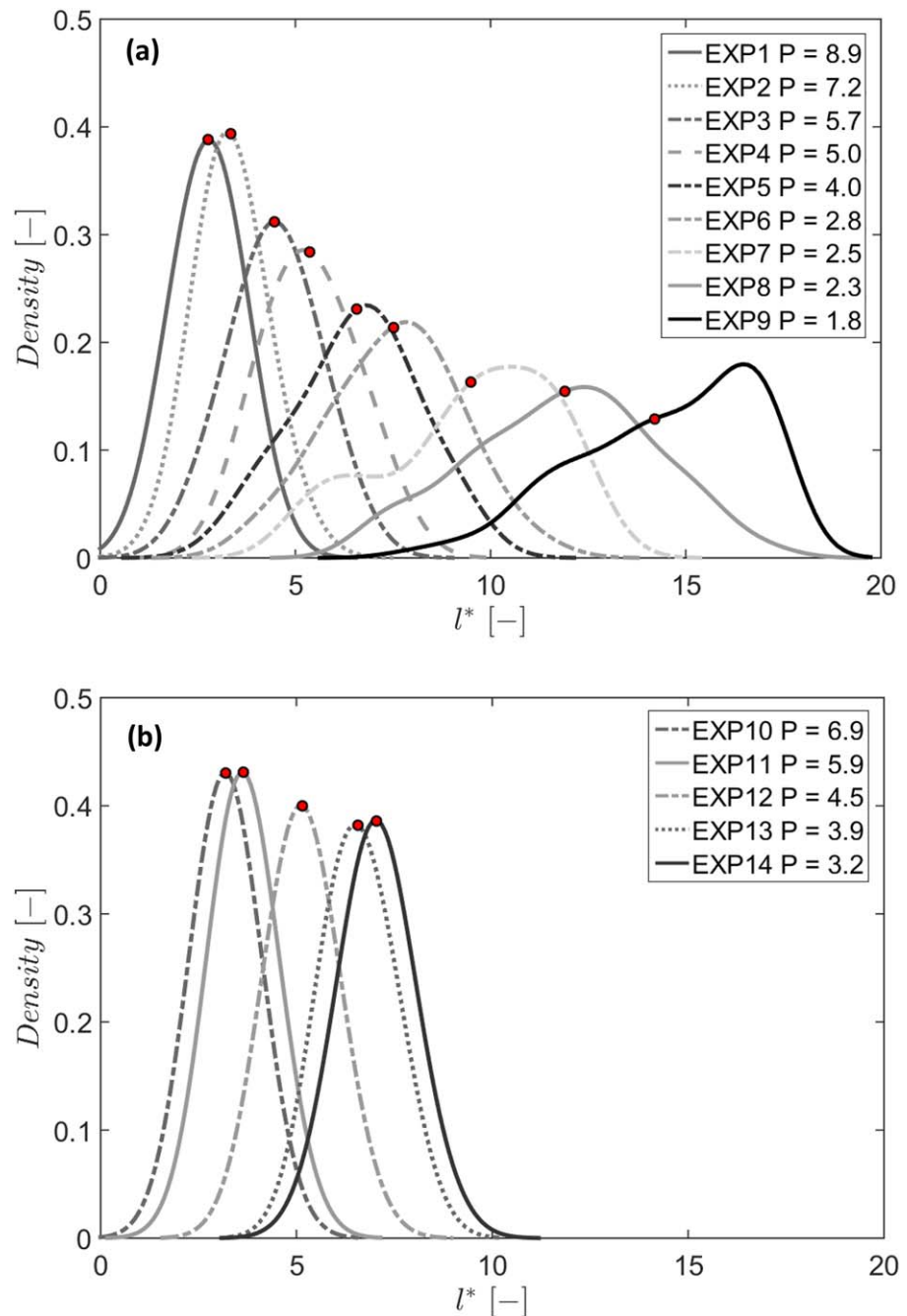


Figure 12. Kernel probability density functions for measured excursion lengths with (a) plastic and (b) sand particles. Red dots indicate mean excursion length for each experiment.

4.2. Comparison of Excursion Length Model With Data

Measured distributions of particle excursion lengths discussed in the previous section are used here for verification of the excursion length model in the $l^*(P, D^*)$ parameter framework (see section 2.1). Figure 13 shows profiles of l^* as a function of Rouse number corresponding to minimum and maximum D^* values of the experimental framework (see Table 1 and Figure 8). Red triangles and green squares indicate mean excursion lengths for experiments with plastic particles and sand particles, respectively. The error bars correspond to measured standard deviations of each distribution (Table 3). The predicted trend of linearly increasing excursion lengths with decreasing Rouse numbers is consistent with measured excursion lengths across a wide range of Rouse numbers ($P=1.8-8.9$). Furthermore, all data points are observed to fit within

Table 3. Summary of Experimental Results

Parameter	Experiments With Plastic Grains									Experiments With Quartz Grains				
	EXP1	EXP2	EXP3	EXP4	EXP5	EXP6	EXP7	EXP8	EXP9	EXP10	EXP11	EXP12	EXP13	EXP14
Relative grain roughness $D^* \times 10^{-2}$	1.55	1.24	1.55	1.55	1.24	1.13	0.79	0.67	0.47	0.45	0.45	0.33	0.33	0.29
Rouse number P	8.9	7.2	5.7	5.0	4.0	2.8	2.5	2.3	1.8	6.9	5.9	4.5	3.9	3.2
Mean dimensionless excursion length l^*	2.76	3.35	4.46	5.37	6.56	7.52	9.56	11.9	14.2	3.19	3.65	5.14	6.58	7.05
Standard deviation σ (l^*)	0.61	0.63	0.98	1.08	1.54	1.65	2.15	2.38	2.63	0.46	0.47	0.59	0.63	0.67

the predicted range of excursion lengths with no significant difference between measured excursion lengths with plastic and sand particles.

Although in the present study particle motion and trajectories were measured across a wide range of flow conditions ($P=1.8-8.9$), due to instrumental and flume limitations, we were not able to reach flow conditions fully dominated by turbulence with minimal contributions from gravitational settling ($P < 0.8$, see section 4.1). Future research should address this if possible and provide distributions of quantities describing particle motion to further constrain the continuous model presented here.

4.3. Connections to Granular Mechanics

As outlined in the Introduction, probabilistic approaches to sediment transport have received significant attention in recent years, with particular interest in measuring distributions of quantities describing particle motion, namely particle velocities, acceleration, travel lengths, and travel times. The focus so far has been primarily limited to bed load particle motion under low to moderate flow conditions. Recent experimental works involve quantification of bed load particle flux and particle diffusion by measuring joint distributions of particle hop lengths and travel times, and by identifying relationships between these [e.g., Roseberry et al., 2012; Fathel et al., 2015 and references therein]. However, there is a growing interest in extending probabilistic approaches to suspended particle motion under high flow conditions. It is also commonly argued that there is no inherent physical difference between saltating bed load and suspended load, and that, in reality, all sediment transport lies along a continuum of travel distances and velocities [e.g., Parsons et al., 2015]. As joint distributions of particle travel lengths and travel times provide knowledge of particle

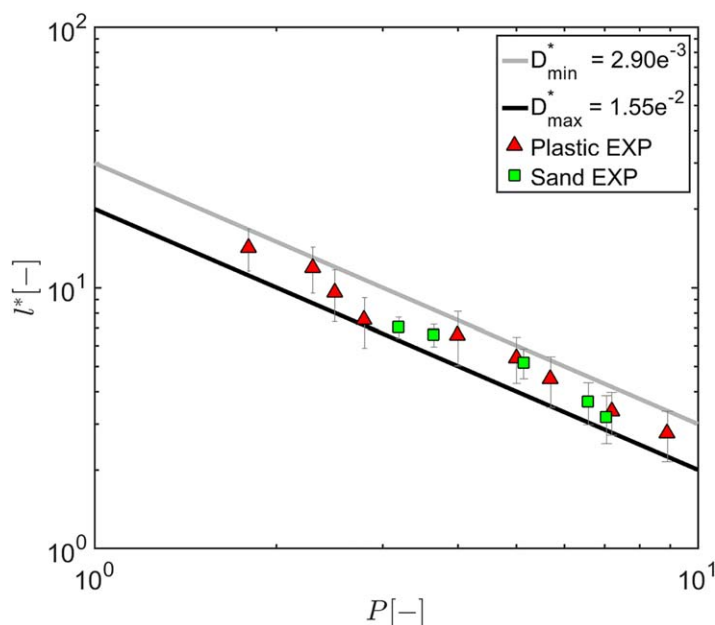


Figure 13. Selected profiles from the continuous particle travel length model for experimentally tested range of relative grain roughness D^* values (Table 2). Red triangles are mean particle excursion lengths obtained from experiments with plastic particles and green squares show mean excursion lengths for sand experiments.

flux and particle diffusion under unsteady conditions, Roseberry et al. [2012] emphasized the need to measure these distributions for a wide range of flow and sediment conditions. This was not yet possible primarily due to the large distances that suspended particles travel once they are picked up from the bed. With the experimental methods and techniques developed in this study, exact particle motion can be measured over relatively large distances including distributions of particle velocities, acceleration, travel lengths, and travel times. In addition, different physical processes can be studied and quantified for suspended particles such as collision-rebound of grains with the bed, hydrodynamic lift forces, and turbulence effects on grains, grain lift-off,

and impact angle at the bed and rotation (Magnus force). This will allow development of probabilistic-based sediment transport models that are likely to be valid across a wider range of flow conditions than hitherto.

4.4. Applications for Bed Form Modeling

For modeling many unsteady morphodynamic problems, knowledge of mean particle motion and travel lengths are required as is information about the distribution of particle lengths. An examples is the class of models describing the growth and instability of bed forms, in particular regime transition from dune to upper stage plane bed [e.g., *Giri and Shimizu, 2006; Shimizu et al., 2009; Nelson et al., 2011; Naqshband et al., 2015; Van Duin, 2015; Yamaguchi et al., 2015*]. Nonequilibrium sediment transport is modeled within these studies by entrainment and deposition functions related to each other through a lag distance. This lag is a function of mean particle travel length and is set constant for a certain flow condition. Because information about the variation of particle travel lengths as a function of flow strength is not available, and in particular this is the case for relatively high flow conditions that are associated with substantial suspension and bed form instability, particle travel length have been assumed to increase linearly with increasing flow strength. As a result, a train of bed forms is modeled with similar wavelengths and natural variation in bed form scale is hardly observed. In addition, lag distances are chosen such that desired morphodynamic changes are achieved without actual details of physical mechanisms governing particle motion and travel lengths. *Jerolmack and Mohrig [2005]* for instance included a white noise term in the Exner equation to account for fluctuations in sediment transport. They found that adding noise resulted in spatial patterns resembling natural bed forms with a continuous range of sizes and shapes as commonly observed in the field. The continuous, validated particle travel length model derived in the present study can be used within this class of models to obtain—for a certain flow condition—distribution of lag distances between particle entrainment and deposition. This approach will allow natural variations in modeled bed form scales based on actual distribution of particle travel lengths.

5. Conclusions

The present study has focused on quantifying particle motions and trajectories across a wide range of flow conditions. In particular, a continuous model was presented that predicts distributions of particle saltation and excursion lengths based on Rouse number, p , and relative grain roughness, D^* . By utilizing a series of eight video cameras in a plexiglass flume—for the first time—direct measurements of the distributions of excursion lengths were obtained. To this end, experiments were carried out in dark under black lights with fluorescent painted plastic and sand particles. Our main findings can be summarized as follows:

1. Particle motion under bed load dominant transport regime is governed by the effect of gravitational forces (settling velocities). Particle trajectories are smooth and regular, and particles are transported only in saltation as soon as they hit the flume bed. Particle trajectories become substantially more irregular under suspended load dominant transport regime due to interactions with random turbulent fluctuation. Consequently, the distance over which particles hit the flume bed becomes much larger.
2. For relatively high Rouse numbers indicating bed load dominant transport regime ($p \geq 2.8$), measured excursion lengths closely follow a Gaussian distribution with distributions being symmetric around their mean values. For $P=2.5$, particle motion is equally subjected to both gravitational and turbulent forces. Consequently, measured excursion lengths exhibit a bimodal distribution with two distinct peaks. As turbulent fluctuations increase and dominate particle motion over gravity ($P < 2.5$), distributions of excursion lengths become unimodal and negative-skewed with mean values deviating from the modes.
3. The predicted trend of linearly increasing excursion lengths with decreasing Rouse numbers is consistent with measured excursion lengths across a wide range of Rouse numbers ($P=1.8-8.9$). Furthermore, measured excursion lengths are observed to fit within the predicted range of excursion lengths with no significant difference between measured excursion lengths with plastic and quartz sand particles.

References

- Abbott, J. E., and J. R. D. Francis (1977), Saltation and suspension trajectories of solid grains in a water stream, *Philos. Trans. R. Soc. London A*, 284(1321), 225–254.
- Ancey, C. (2010), Stochastic approximation of the Exner equation under lower-regime conditions, *J. Geophys. Res.*, 115, F00A11, doi: 10.1029/2009JF001260.

Acknowledgments

We thank the donors of the American Chemical Society Petroleum Research Fund 54492-DN18 and the University of Wyoming School for Energy Resources for partially supporting this research. We also want to thank the Editor (Alberto Montanari), the associate editor (Christophe Ancey), and three unknown reviewers for providing great suggestions and feedback which improved this manuscript. Data supporting analysis and conclusions are available in the supporting information.

- Ancey, C., A. C. Davison, T. Bohm, M. Jodeau, and P. Frey (2008), Entrainment and motion of coarse particles in a shallow water stream down a steep slope, *J. Fluid Mech.*, *595*, 83–114, doi:10.1017/S0022112007008774.
- Andreotti, B., P. Claudin, and O. Pouliquen (2010), Measurements of the aeolian sand transport saturation length, *Geomorphology*, *123*, 343–348.
- Arcement, G. J., and V. Schneider (1989), Guide for selecting Manning's roughness coefficients for natural channels and flood plains, *U.S. Geol. Surv. Water Supply Pap.*, *2339*, 38 p.
- Bagnold, R. A. (1973), The nature of saltation and of bed-load transport, water, *Proc. R. Soc. London, Ser. A*, *332*, 473–504.
- Bathurst, J. C. (2007), Effect of coarse surface layer on bed-load transport, *J. Hydraul. Eng.*, *133*, 1192–1205.
- Bhattacharyya, A., S. P. Ojha, and B. S. Mazumder (2013), Evaluation of the saltation process of bed materials by video imaging under altered bed roughness, *Earth Surf. Processes Landforms*, *38*, 1339–1353, doi:10.1002/esp.3370.
- Bialik, R. J. (2011), Particle–particle collision in Lagrangian modeling of saltating grains, *J. Hydraul. Res.*, *49*(1), 23–31.
- Bialik, R. J. (2015), Lagrangian modelling of saltating sediment transport: A review, in *Rivers-Physical, Fluvial and Environmental Processes*, pp. 427–441, Springer, Cham, Switzerland.
- Bialik, R. J., V. I. Nikora, and P. M. Rowiński (2012), 3D Lagrangian modelling of saltating particles diffusion in turbulent water flow, *Acta Geophys.*, *60*(6), 1639–1660.
- Bridge, J. S., and S. J. Bennett (1992), A model for the entrainment and transport of sediment grains of mixed sizes, shapes and densities, *Water Resour. Res.*, *28*, 337–363.
- Chatanantavet, P., K. X. Whipple, M. A. Adams, and M. P. Lamb (2013), Experimental study on coarse grain saltation dynamics in bedrock channels, *J. Geophys. Res. Earth Surf.*, *118*, 1161–1176, doi:10.1002/jgrf.20053.
- Claudin, P., F. Charru, and B. Andreotti (2011), Transport relaxation time and length scales in turbulent suspensions, *J. Fluid Mech.*, *671*, 491–50.
- Crocker, J. C., and D. G. Grier (1996), Methods of digital video microscopy for colloidal studies, *J. Colloid Interface Sci.*, *179*, 298–310.
- Dade, B. W., and H. E. Huppert (1994), Predicting the geometry of channelized deep-sea turbidites, *Geology*, *22*, 645–648, doi:10.1130/0091-7613022.
- Davy, P., and D. Lague (2009), Fluvial erosion/transport equation of landscape evolution models revisited, *J. Geophys. Res.*, *114*, F03007, doi:10.1029/2008JF001146.
- Drake T. G., R. L. Shreve, W. E. Dietrich, P. J. Whiting, and L. B. Leopold (1988), Bedload transport of fine gravel observed by motion-picture photography, *J. Fluid Mech.*, *192*, 193–217.
- Einstein, H. A. (1950), The bedload function for sediment transportation in open channel flow, *Tech. Bull. 1026*, pp. 1–71, USDA Soil Conserv. Serv., U.S. Dep. of Agric., Washington, D. C.
- Engelund, F., and E. Hansen (1967), *A Monograph on Sediment Transport in Alluvial Streams*, Teknisk Forlag, Copenhagen.
- Fathel, S. L., D. J. Furbish, and M. W. Schmeeckle (2015), Experimental evidence of statistical ensemble behavior in bed load sediment transport, *J. Geophys. Res. Earth Surf.*, *120*, 2298–2317, doi:10.1002/2015JF003552.
- Fernandez-Luque, R., and R. van Beek (1976), Erosion and transport of bedload sediment, *J. Hydraul. Res.*, *14*(2), 127–144.
- Francis, J. R. D. (1973), Experiments on the motion of solitary grains along the bed of a water stream, *Proc. R. Soc. London, Ser. A*, *332*, 443–471.
- Furbish, D. J., P. K. Haff, J. C. Roseberry, and M. W. Schmeeckle (2012a), A probabilistic description of the bed load sediment flux: 1. Theory, *J. Geophys. Res.*, *117*, F03031, doi:10.1029/2012JF002352.
- Furbish, D. J., A. E. Ball, and M. W. Schmeeckle (2012c), A probabilistic description of the bed load sediment flux: 4. Fickian diffusion at low transport rates, *J. Geophys. Res.*, *117*, F03034, doi:10.1029/2012JF002356.
- Furbish, D. J., M. W. Schmeeckle, R. Schumer, and S. L. Fathel (2016), Probability distributions of bed load particle velocities, accelerations, hop distances, and travel times informed by Jaynes's principle of maximum entropy, *J. Geophys. Res. Earth Surf.*, *121*, 1373–1390, doi:10.1002/2016JF003833.
- Garcia, M. (1994), Depositional turbidity currents laden with poorly sorted sediment, *J. Hydraul. Eng.*, *120*, 1240–1263, doi:10.1061/(ASCE)0733-9429(1994)120:11(1240).
- Giri, S., and Y. Shimizu (2006), Computation of sand dune migration with free surface flow, *Water Resour. Res.*, *42*, W10422, doi:10.1029/2005WR004588.
- Hendershot, M. L., J. G. Venditti, R. W. Bradley, R. A. Kostaschuk, M. Church, and M. A. Allison (2016), Response of low-angle dunes to variable flow, *Sedimentology*, *63*, 743–760, doi:10.1111/sed.12236.
- Hergault, V., P. Frey, F. Métivier, C. Barat, C. Ducottet, T. Böhm, and C. Ancey (2010), Image processing for the study of bedload transport of two-size spherical particles in a supercritical flow, *Exp. Fluids*, *49*(5), 1095–1107.
- Heyman, J. (2014), A study of the spatiotemporal behaviour of bed load transport rate fluctuations, PhD thesis, Ecole Polytech. Fed. de Lausanne, Lausanne, Switzerland.
- Heyman, J., H. B. Ma, F. Mettra, and C. Ancey (2014), Spatial correlations in bed load transport: Evidence, importance, and modelling, *J. Geophys. Res. Earth Surf.*, *119*, 1751–1767, doi:10.1002/2013JF003003.
- Hu, C., and Y. Hui (1996), Bed-load transport I: Mechanical characteristics, *J. Hydraul. Eng.*, *122*, 245–254.
- Jerolmack, D. J., and D. Mohrig (2005), A unified model for subaqueous bed form dynamics, *Water Resour. Res.*, *41*, W12421, doi:10.1029/2005WR004329.
- Jopling, A. V. (1963), Hydraulic studies on the origin of bedding, *Sedimentology*, *2*, 115–121.
- Julien, P. Y. (1994), *Erosion and Sedimentation*, Colo. State Univ., Fort Collins.
- Lajeunesse, E., L. Malverti, and F. Charru (2010), Bed load transport in turbulent flow at the grain scale: Experiments and modeling, *J. Geophys. Res.*, *115*, F04001, doi:10.1029/2009JF001628.
- Lamb, M. P., B. McElroy, B. Kopriva, J. Shaw, and D. Mohrig (2010), Linking river-flood dynamics to hyperpycnal-plume deposits: Experiments, theory, and geological implications, *Geol. Soc. Am. Bull.*, *122*(9/10), 1389–1400, doi:10.1130/B30125.1.
- Lee, H. Y., and I. S. Hsu (1994), Investigation of saltating particles motions, *J. Hydraul. Eng.*, *120*(7), 831–845.
- Lee, H. Y., and I. S. Hsu (1996), Particle spinning motion during saltating process, *J. Hydraul. Eng.*, *122*(10), 587–590.
- Lee, H. Y., Y. Chen, J. You, and Y. Lin (2000), Investigations of continuous bed load saltating process, *J. Hydraul. Eng.*, *126*(9), 691–700.
- Lee, H. Y., J. Y. You, and Y. T. Lin (2002), Continuous saltating process of multiple sediment particles, *J. Hydraul. Eng.*, *128*(4), 443–450.
- Lee, H. Y., Y. T. Lin, Y. H. Chen, J. Y. You, and H. W. Wang (2006), On three-dimensional continuous saltating process of sediment particles near the channel bed, *J. Hydraul. Res.*, *44*(3), 374–389.
- Lukerchenko, N., Y. Kvurt, A. Kharlamov, Z. Chara, and P. Vlasak (2008), Experimental evaluation of the drag force and drag torque acting on a rotating spherical particle moving in fluid, *J. Hydrol. Hydromech.*, *56*(2), 88–94.

- Mazumder, B. S., A. Bhattacharyya, and O. P. Satya (2008), Near bed particle motion due to turbulent flow using image processing technique, *J. Flow Visual. Image Process.*, *14*, 1–15.
- Meyer-Peter, E., and R. Muller (1948), Formulas for bedload transport, in *Proceedings of 2nd International IAHR Congress*, pp. 39–64, Int. Assoc. of Hydraul. Res., Stockholm.
- Mohrig, D., and J. D. Smith (1996), Predicting the migration rates of subaqueous dunes, *Water Resour. Res.*, *32*, 3207–3217, doi:10.1029/96WR01129.
- Naqshband, S., and B. McElroy (2016), Sediment transport at grain scale: A review, future research and morphological implications, in *Proceedings of the International Conference on Fluvial Hydraulics (River Flow)*, St. Louis, USA, 11–14 July, edited by G. Constantinescu, M. Garcia, and D. Hanes, pp. 914–919, CRC Press, London, U. K.
- Naqshband S., J. S. Ribberink, and S. J. M. H. Hulscher (2014), Using both free surface effect and sediment transport mode parameters in defining the morphology of river dunes and their evolution to upper stage plane beds, *J. Hydraul. Eng.*, *140*(6), 06014010, doi:10.1061/(ASCE)HY.1943-7900.0000873.
- Naqshband, S., O. J. M. van Duin, J. S. Ribberink, and S.J.M.H. Hulscher (2015), Modelling river dune development and dune transition to upper stage plane bed, *Earth Surf. Processes Landforms*, *41*, 323–335, doi:10.1002/esp.3789.
- Nelson, J. M., B. L. Logan, P. J. Kinzel, Y. Shimizu, S. Giri, R. L. Shreve, and S. R. McLean (2011), Bed form response to flow variability, *Proc. Earth Surf. Landforms*, *36*, 1938–1947.
- Niño, Y., and M. Garcia (1994), Gravel saltation 2: Modelling, *Water Resour. Res.*, *30*, 1915–1924.
- Niño, Y., and M. Garcia (1998), Experiments on saltation of sand in water, *J. Hydraul. Eng.*, *124*, 1014–1025.
- Niño, Y., M. Garcia, and L. Ayala (1994), Gravel saltation 1: Experiments, *Water Resour. Res.*, *30*, 1907–1914.
- Paola, C., and V. R. Voller (2005), A generalized Exner equation for sediment mass balance, *J. Geophys. Res.*, *110*, F04014, doi:10.1029/2004JF000274.
- Parker, G. (1978), Self-formed straight rivers with equilibrium banks and mobile bed. Part 1. The sand–silt river, *J. Fluid Mech.*, *89*, 109–125.
- Parker, G., M. Garcia, Y. Fukushima, and W. Yu (1987), Experiments on turbidity currents over an erodible bed, *J. Hydraul. Res.*, *25*, 123–147.
- Parsons, A. J., J. Cooper, and J. Wainwright (2015), What is suspended sediment?, *Earth Surf. Processes Landforms*, *40*, 1417–1420, doi:10.1002/esp.3730.
- Roseberry, J. C., M. W. Schmeeckle, and D. J. Furbish (2012), A probabilistic description of the bed load sediment flux: 2. Particle activity and motions, *J. Geophys. Res.*, *117*, F03032, doi:10.1029/2012JF002353.
- Rowiński, P.M. (1995), Transport of solid particles in turbulent water flow [in Polish], PhD thesis, Inst. of Geophys., Pol. Acad. of Sci., Warsaw.
- Schmeeckle, M. W., J. M. Nelson, and J. P. Bennett (2001), Interparticle collision of natural sediment grains in water, *Water Resour. Res.*, *37*, 2377–2391, doi:10.1029/2001WR000531.
- Sekine, M., and H. Kikkawa (1992), Mechanics of saltating grains. II, *J. Hydraul. Eng.*, *118*(4), 536–558.
- Seminara, G., L. Solari, and G. Parker (2002), Bed load at low Shields stress on arbitrarily sloping beds: Failure of the Bagnold hypothesis, *Water Resour. Res.*, *38*(11), 1249, doi:10.1029/2001WR000681.
- Shimizu, Y., S. Giri, I. Yamaguchi, and J. Nelson (2009), Numerical simulation of dune-flat bed transition and stage-discharge relationship with hysteresis effect, *Water Resour. Res.*, *45*, W04429, doi:10.1029/2008WR006830.
- Straub, K.M., and D. Mohrig (2008), Quantifying the morphology and growth of levees in aggrading submarine channels, *J. Geophys. Res.*, *113*, F03012, doi:10.1029/2007JF000896.
- Van Duin, O. J. M. (2015), Sediment transport processes in dune morphology and the transition to upper-plane stage bed, PhD thesis, Univ. of Twente, Enschede, Netherlands.
- Van Rijn, L. C. (1984), Sediment pick-up functions, *J. Hydraul. Eng.*, *110*, 1494–1502.
- Van Rijn, L. C. (1993), *Principles of Sediment Transport in Rivers, Estuaries and Coastal Seas*, 335 p., AQUA Publ., Amsterdam.
- White, B. R., and J. Schulz (1977), Magnus effect in saltation, *J. Fluid Mech.*, *81*(3), 497–512.
- Wiberg, P. L., and J. D. Smith (1987), Calculation of the critical shear stress for motion of uniform and heterogeneous sediments, *Water Resour. Res.*, *23*, 1471–1480.
- Wilcock, P. R. (2001), Toward a practical method for estimating sediment-transport rates in gravel bed-rivers, *Earth Surf. Processes Landforms*, *26*, 1395–1408.
- Wright, S., and G. Parker (2004), Density stratification effects in sand-bed rivers, *J. Hydraul. Eng.*, *130*, 783–795.
- Yalin, M., and A. Ferreira da Silva (2001), *Fluvial Processes*, Int. Assoc. of Hydraul. Eng. and Res., Delft, Netherlands.
- Yamaguchi, S., S. Giri, J. M. Nelson, Y. Shimizu, and J. Funaki (2015), Numerical simulations on response of dune bed forms to flow variability, *J. Jpn. Soc. Civ. Eng.*, *71*, 1015–1020.
- Zou, X. Y., H. Cheng, C. L. Zhang, and Y.Z. Zhao (2007), Effects of the Magnus and Saffman forces on the saltation trajectories of sand grain, *Geomorphology*, *90*(1–2), 11–22.